Tunnel-injection GaN quantum dot ultraviolet light-emitting diodes

Jai Verma, Prem Kumar Kandaswamy, Vladimir Protasenko, Amit Verma, Huili Grace Xing, and Debdeep Jena[a)]
Department of Electrical Engineering, University of Notre Dame, Indiana 46556, USA

(Received 17 September 2012; accepted 14 January 2013; published online 28 January 2013)

We demonstrate a GaN quantum dot ultraviolet light-emitting diode that uses tunnel injection of carriers through AlN barriers into the active region. The quantum dot heterostructure is grown by molecular beam epitaxy on AlN templates. The large lattice mismatch between GaN and AlN favors the formation of GaN quantum dots in the Stranski-Krastanov growth mode. Carrier injection by tunneling can mitigate losses incurred in hot-carrier injection in light emitting heterostructures. To achieve tunnel injection, relatively low composition AlGaN is used for n- and p-type layers to simultaneously take advantage of effective band alignment and efficient doping. The small height of the quantum dots results in short-wavelength emission and are simultaneously an effective tool to fight the reduction of oscillator strength from quantum-confined Stark effect due to polarization fields. The strong quantum confinement results in room-temperature electroluminescence peaks at 261 and 340 nm, well above the 365 nm bandgap of bulk GaN. The demonstration opens the doorway to exploit many varied features of quantum dot physics to realize high-efficiency short-wavelength light sources. © *2013 American Institute of Physics*. [http://dx.doi.org/10.1063/1.4789512]

Robust and compact semiconductor ultraviolet (UV) light emitting sources operating in the wavelength range of 250–350 nm have attracted considerable interest for potential applications in sterilization, aerosol detection, and water purification. Light emitting diodes (LEDs) and laser diodes (LDs) containing direct bandgap Al(GaIn)N alloy active regions are being actively pursued for this need. UV LEDs operating in the wavelength range between 380 and 210 nm have been reported,[1,2] yet the efficiency and the consequent output power is observed to plummet from 400 mW ($\lambda = 375$ nm) to 0.3 mW ($\lambda = 250$ nm) with decreasing wavelength. The high external quantum efficiency (EQE) numbers obtained for InGaN based blue LEDs and LDs are not achieved in the case of high Al containing Al(GaIn)N alloys. When compared to InGaN based visible LEDs, the severe degradation in performance of Al containing UV LEDs is due to several factors.

The III-nitride semiconductor heterostructures for the UV LEDs have been predominantly grown on sapphire due to the limited availability of native AlN substrates which offer lower lattice mismatch. The lattice mismatch results in high threading dislocation (TD) densities of the order of $>10^8\,\mathrm{cm}^{-2}$. In quantum well (QW) structures the carriers are confined in one direction (the growth direction) but are free to move in the other two directions (the growth plane). The TDs act as non-radiative recombination sites where the injected electrons and holes can recombine, even in QW structures. Recently, the internal quantum efficiency (IQE) has been increased from 20% to 60%, contributing to an external quantum efficiency (EQE) of 10%, by reducing the TD density below $2 \times 10^8\,\mathrm{cm}^{-2}$ in UV LED structures.[3] Thus, TDs play a strong role in reducing the IQE of UV LEDs unlike the InGaN based visible LEDs, where In segregation provides carrier confinement like a quantum dot. Additionally, when the Al content is increased in the Al(GaIn)N beyond a Al mole fraction of 0.3 in the active region, the valence band structure changes in a manner that promotes emission of transverse magnetic (TM: E||c) polarized light, accompanied by a reduction in IQE.[4,5] The in-plane emission is problematic for efficient light extraction from the surface. This effect is not observed in InGaN LEDs, and the problem can be overcome in UV LEDs by designing asymmetric AlGaN QWs embedded with very thin GaN layers of the order of 1–2 MLs.[6] Superimposed on the above issues is the quantum confined Stark effect (QCSE) induced by the strong spontaneous and piezoelectric polarization in III-nitrides,[9] which reduces the oscillator strength of optical transitions, lowering the radiative recombination rates.[10]

The thermally excited free-carrier concentration decreases sharply with increasing Al content due to large ionization energies of acceptors ($E_A \sim 630$ meV for AlN:Mg) and donors ($E_D \sim 282$ meV for AlN:Si).[7,8] Visible LED heterostructures utilize GaN cladding layers that boast relatively low dopant ionization energies than the UV counterparts. The GaN cladding layers can be doped heavily and have a larger bandgap than the active region. This leads to better carrier injection and confinement with minimal reabsorption of the emitted light. The cladding layers of UV LEDs must also be transparent to the energy of emitted photons, requiring high Al-containing Al(GaIn)N alloys in the n- and p-type contact layers. The high dopant activation energy reduces the carrier concentration which severely limits the injection efficiency. Besides, in conventional LED design the carriers are injected above the barrier (hot carriers) into the QW, which results in energy loss by phonon emission, Auger recombination, and carrier leakage.

To overcome the above issues of non-radiative recombination, valence band asymmetry, hot carrier injection, and low doping in high Al content III-nitride layers, we propose and demonstrate GaN/AlN QD UV LEDs that use tunnel injection and relatively low Al-composition cladding layers.

[a)]Electronic mail: djena@nd.edu.

 © 2013 American Institute of Physics

Downloaded 28 Jan 2013 to 129.74.113.138. Redistribution subject to AIP license or copyright; see http://apl.aip.org/about/rights_and_permissions

The formation of QDs in the SK growth mode is favored by a large lattice mismatch, such as between GaN and AlN (2.4%). Replacing QWs with QDs provides 3-dimensional carrier confinement in the active region increasing the radiative recombination, since carrier capture into dots keeps them away from non-radiative sites at dislocations. Though high Al composition AlGaN does not have enough lattice mismatch with AlN to form QDs, growth of InAlGaN/AlN QDs by Stranski-Krastanov (SK) and anti-surfactant methods have been demonstrated with peak emission wavelengths in the UV[11] and the visible[12] regions. The emission wavelength of QDs can be tailored to shorter wavelengths by reducing the height of the QDs.[13] This aids in achieving short wavelengths at relatively low Al composition than in QWs. As a consequence, the valence band structure modification induced by high Al content is lowered, and due to better electron-hole overlap QCSE is significantly reduced, resulting in enhanced radiative recombination efficiency.[14] Tunnel injection of carriers into InGaN QDs was recently demonstrated by Bhattacharya *et al.*[15] Such tunnel-injection LEDs exhibit reduced efficiency droop in InGaN green LEDs by suppressing the detrimental effects of hot carrier injection.

To achieve optimal tunnel injection in our structure, we use AlGaN n- and p-type cladding layers with bandgap just above the emission wavelength of QDs to minimize reabsorption of the emitted photons. This feature can enable improved n- and p-type doping efficiency, because the dopant activation energies in the low-Al content AlGaN cladding layers is significantly lower. Therefore, carrier injection efficiency can be improved dramatically. Besides, the spatial distribution of electron and hole wavefunctions in pyramidal GaN QDs,[16] as well as the thin AlN barrier, promotes tunneling transport of carriers (electrons and holes)[17] despite the large effective mass of holes. As a result of strong quantum confinement the QD eigenvalues are shifted to higher energies resulting in short wavelength emission. The corresponding eigenfunctions extend deep into the barriers promoting tunneling transport, along with the available phase space due to QD size distribution. In addition, the much speculated phonon bottleneck[18] problem associated with QD systems can be overcome, because the carriers can be injected directly into the lowest energy state of the QD. Therefore, QD based active regions and tunnel injection offer potential solutions to a number of problems associated with high Al content UV LED heterostructures.

Figure 1(a) shows the structure of the GaN/AlN QD UV LED. The heterostructure is grown on commercially available AlN-on-sapphire templates by plasma-assisted molecular beam epitaxy (MBE). A 100 nm AlN nucleation layer was grown with III/V ratio ~1 to move away from the MOCVD grown AlN template. A 285 nm Si-doped AlGaN n-cladding layer was deposited in the metal-rich growth regime. A $M = 8$ period self-assembled GaN/AlN QD active layer stack was then grown at 730 °C under Ga-limited condition and III/V ratio ~0.95. Finally, a 80 nm Mg doped p-type AlGaN layer was deposited at 630 °C to complete the QD LED structure. The doping densities were Si: 5×10^{19} cm^{-3} and Mg: 4×10^{19} cm^{-3} as obtained from comparative SIMS data of Si and Mg doped GaN. The growth rate was ~160 nm/h. Atomic force microscopy (AFM) scans of uncapped QDs showed bimodal size distribution of QDs with a dot density of $n_{dot} \sim 4 \times 10^8$ cm^{-2} and $\sim 5 \times 10^9$ cm^{-2} for thick and thin QDs, respectively. A similar bimodal size distribution had been observed earlier with larger GaN QDs grown under Ga-limited conditions.[19] The Al compositions of the n- and p-cladding layers were measured by fitting the measured and simulated X-ray diffraction (XRD) triple-axis ω-2θ scans. They were inferred to be $Al_{0.45}Ga_{0.55}N$ for the n-layer, and $Al_{0.50}Ga_{0.50}N$ for the p-layer.

Figure 1(b) shows the calculated energy band diagram of the active region under zero bias. The large barrier height (~1.25 eV for electrons and ~0.25 eV for holes) between the AlN barriers and the AlGaN contact layers prevents the conventional injection of carriers over the barrier into the active region, whereas the small thickness allows for tunneling injection. A wedge was cut from the grown heterostructure using focused ion beam (FIB) for transmission electron microscope (TEM) analysis. The *Z*-contrast scanning transmission electron micrograph (STEM) is shown in Figure 1(c). The QD thickness is $t_{dot} \sim 0.55$ nm, and the AlN barrier thickness is $t_b \sim 2.8$ nm. The image also shows the entire QD LED heterostructure with the 8-period AlN barrier/GaN QD stack active region, the n- and p-AlGaN layers, and the AlN substrate.

Photoluminescence (PL) measurements were was performed on the GaN QDs in the AlN matrix and the AlGaN layer, grown under similar conditions as the complete QD

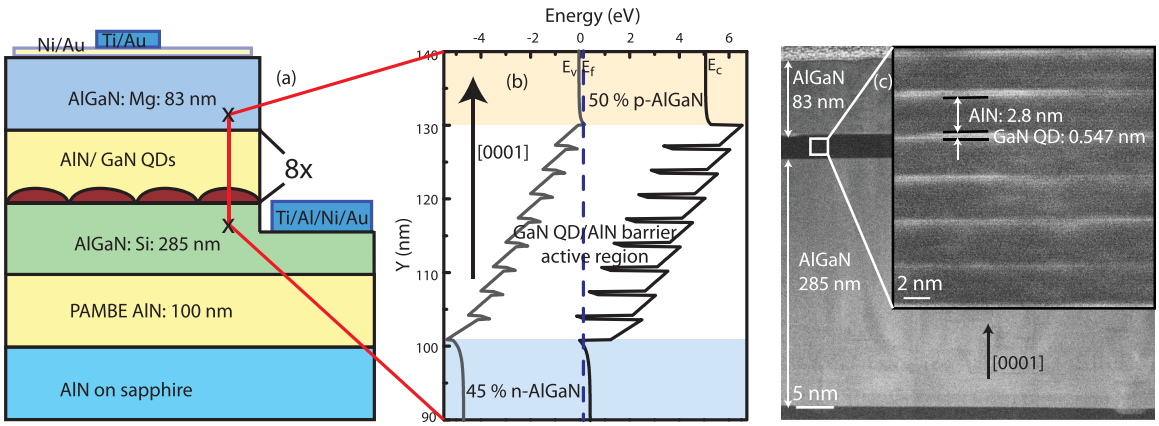

FIG. 1. (a) Tunnel injection GaN quantum dot LED structure with contact metals, (b) energy band diagram of the UV-LED active region and the contact layers at zero bias, and (c) STEM scan of the UV-LED structure showing 8-period GaN QDs embedded in AlN barriers.

Downloaded 28 Jan 2013 to 129.74.113.138. Redistribution subject to AIP license or copyright; see http://apl.aip.org/about/rights_and_permissions

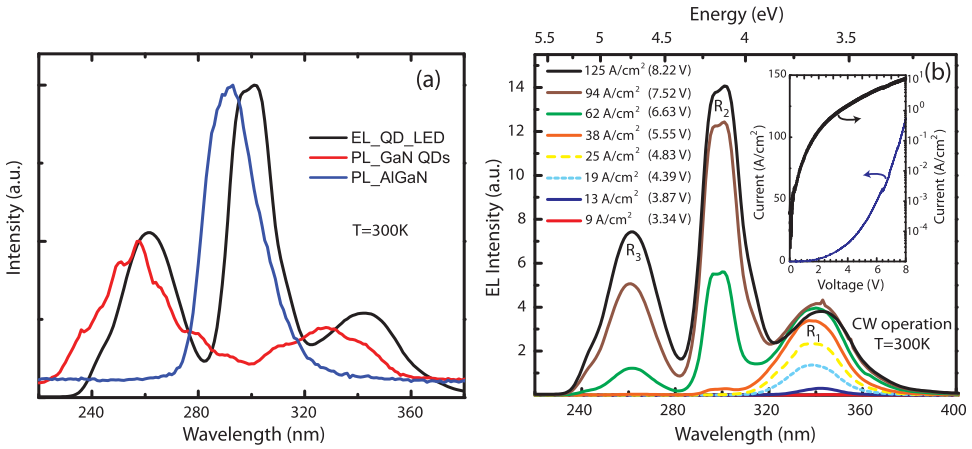

FIG. 2. (a) Photoluminescence spectrum of the GaN QDs and AlGaN layer measured at room temperature, superimposed with the electroluminescence spectrum from the QD UV LED. The PL spectrum shows a peak at 257 nm from the 2 ML thick GaN QD, 328 nm from the comparatively thicker GaN QDs, and 293 nm from AlGaN layer with similar composition as in the p-AlGaN of QD LED structure. (b) Electroluminescence spectrum of GaN/AlN QD UV LEDs at various injection current densities. The EL spectrum shows emission peaks at 301 nm (R_2), 341 nm (R_1), and 261 nm (R_3). (b) Inset: current-voltage characteristics for the QD LED.

LED structure, by exciting them with an (F_2 based) excimer laser with photon energy $\lambda_{exc} = 157$ nm. The measured room-temperature PL spectra are shown in Figure 2(a). The PL peak at 293 nm corresponds to emission from the AlGaN layer, the 257 nm peak corresponds to the 2 monolayer thick GaN QDs, and the 328 nm peak corresponds to comparatively thicker QDs.[13] The QD LED structure was processed into a diode by etching 170 nm down to the n-type layer using Cl_2 based plasma in a reactive ion etcher (RIE). Electron-beam deposited Ti/Al/Ni/Au (20/100/40/50 nm) metal stack was used as the n-type contact layer. Ni/Au (5/5 nm) was deposited as a transparent current spreading layer on the p-type $Al_{0.50}Ga_{0.50}N$ layer. Thicker Ti/Au (20/100 nm) contact metals were deposited over a small area of the transparent metal layer to allow electrical probing and light extraction from the thinner regions.

QD LEDs of mesa size $200 \times 400\ \mu m^2$ were characterized for room temperature electroluminescence (EL). The EL spectrum shown in Figure 2(b) exhibits a peak emission at $\lambda_1 \sim 341$ nm at injection current of $J_{inj} \sim 25\ A/cm^2$. On increasing the injection current to $62\ A/cm^2$, emission was obtained at two additional peak wavelengths $\lambda_2 \sim 301$ nm and $\lambda_3 \sim 261$ nm. Figures 3(a) and 3(b) show schematic energy band diagrams of GaN QDs of 2 different thicknesses embedded within AlN barrier layers. The $\lambda_1 \sim 341$ nm peak is attributed to emission (R_1) from quantized state of the 4 monolayer (ML) thick GaN QDs which are present along with the smaller height QDs,[13] the 261 nm emission (R_3) is attributed to the emission from the 2–3 ML thick QDs. The intense 301 nm emission (R_2) is attributed to the emission from the p-AlGaN layer either by carrier recombination in AlGaN resulting from carrier spillover and/or excitation of p-AlGaN by the 261 nm emission (R_3) coming from the 2–3 ML thick QDs. This is supported by Figure 2(a) which shows the QD LED EL spectrum superimposed with PL spectra of GaN QDs and the AlGaN layer.

Figure 3(c) shows the evolution of peak emission intensities corresponding to the three different peak wavelengths with increasing injection current density. At low injection currents the carriers are able to tunnel into the large QDs which have lower energy levels. Therefore, the emission is at longer wavelength of $\lambda_1 \sim 341$ nm (transition R_1). With increasing current the $\lambda_1 \sim 341$ nm peak intensity saturates, while the R_2 and R_3 emission from p-AlGaN and smaller QDs, respectively, increases. The $\lambda_2 \sim 301$ nm peak intensity crosses the 341 nm peak intensity at $J_{inj} \sim 62\ A/cm^2$. The inset of Figure 3(c) shows the biased GaN QD UV-LED pumping a piece of paper as seen under the microscope.

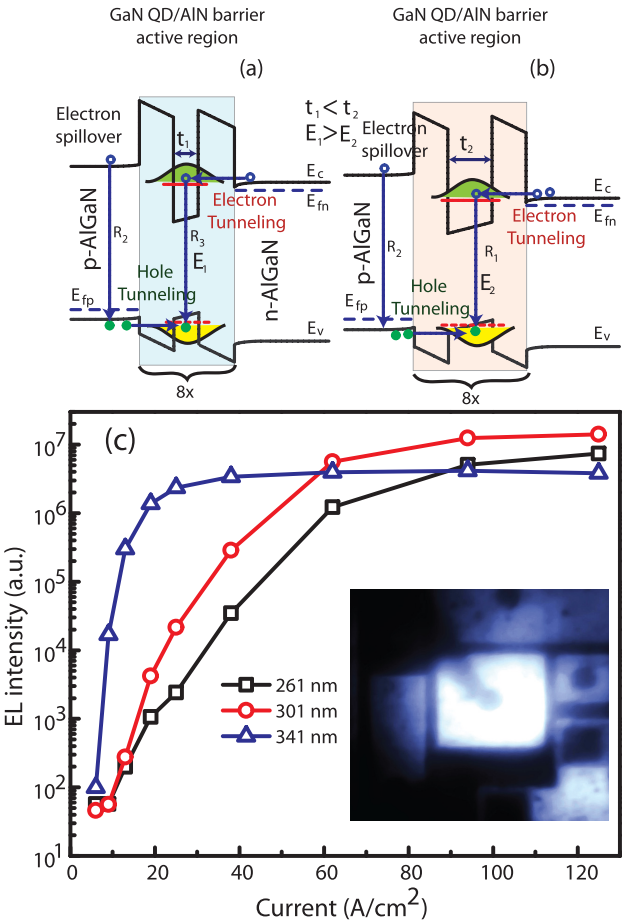

FIG. 3. Schematic energy band diagram of the GaN/AlN QD active regions under bias showing the tunneling transport and recombination mechanisms in (a) thin and (b) thick QDs, and the AlGaN cladding layer. For low injection currents the carriers first tunnel into the thick QD which has lower ground-state energy levels, and the emission is at 341 nm (R_1, E_2: emission energy). On increasing the injected current the higher energy levels in thin QDs are accessed, resulting in 261 nm (R_3, E_1: emission energy). The 301 nm peak emission originates from the AlGaN layer either by carrier recombination from excess carrier spillover and/or excitation by the 261 nm peak emission. (c) The evolution of emission peak intensities with injection current density. The 301 nm and 341 nm peak intensity crossover takes place at ~62 A/cm² whereas the 261 nm and 341 nm peak intensity crossover takes place at ~94 A/cm². (c) Inset: QD UV LED exciting paper kept underneath to produce visible light.

Downloaded 28 Jan 2013 to 129.74.113.138. Redistribution subject to AIP license or copyright; see http://apl.aip.org/about/rights_and_permissions

In conclusion, carrier recombination in QDs and carrier injection by tunneling offers potential solutions to the major problems encountered in deep-UV LEDS such as doping, sensitivity to defects, and valence band asymmetry. In this work, we have proposed a method to realize deep-UV LEDs by taking advantage of GaN quantum dot active regions surrounded by AlN barriers. Carriers are tunnel-injected into the dots from relatively low composition AlGaN regions that facilitate efficient doping. The tunnel-injection process reduces losses incurred in hot-carrier injection into the active regions. Furthermore, the lower valence band offset offers lower tunneling barriers for holes, making up for its heavier mass. This is the demonstration of the feasibility of the basic idea, and many of the advantages discussed have to be carefully studied in the future. Nevertheless, since the experimental demonstration indicates that the design is sound, light emission can be enhanced in the future by fine-tuning the heterostructure design and adopting polarization-induced doping for shorter wavelength UV-LEDs.

[1]A. Khan, K. Balakrishnan, and T. Katona, Nat. Photonics **2**, 77 (2008).
[2]M. Kneissl, T. Kolbe, C. Chua, V. Kueller, N. Lobo, J. Stellmach, A. Knauer, H. Rodriguez, S. Einfeldt, Z. Yang, N. M. Johnson, and M. Weyers, Semicond. Sci. Technol. **26**, 014036 (2011).
[3]M. Shatalov, W. Sun, A. Lunev, X. Hu, A. Dobrinsky, Y. Bilenko, J. Yang, M. Shur, R. Gaska, C. Moe, G. Garrett, and M. Wraback, Appl. Phys. Express **5**, 082101 (2012).
[4]K. B. Nam, J. Li, M. L. Nakarmi, J. Y. Lin, and H. X. Jiang, Appl. Phys. Lett. **84**, 5264 (2004).
[5]A. A. Yamaguchi, Phys. Status Solidi C **5**, 2364 (2008).
[6]J. Zhang, H. Zhao, and N. Tansu, Proc. SPIE **8277**, 82770J (2012).
[7]P. Kozodoy, H. Xing, S. P. DenBaars, U. K. Mishra, A. Saxler, R. Perrin, S. Elhamri, and W. C. Mitchel, J. Appl. Phys. **87**, 1832 (2000).
[8]Y. Taniyasu, M. Kasu, and T. Makimoto, Nature (London) **441**, 325 (2006).
[9]F. Bernardini and V. Fiorentini, Phys. Status Solidi A **190**, 65 (2002).
[10]P. Waltereit, O. Brandt, A. Trampert, H. T. Grahn, J. Menniger, M. Ramsteiner, M. Reiche, and K. H. Ploog, Nature (London) **406**, 865 (2000).
[11]H. Hirayama and F. Fujikawa, Phys. Status Solidi C **5**, 2312 (2008).
[12]T. D. Moustakas, T. Xu, C. Thomidis, A. Y. Nikiforov, L. Zhou, and D. J. Smith, Phys. Status Solidi A **205**, 2560 (2008).
[13]J. Renard, P. K. Kandaswamy, E. Monroy, and B. Gayral, Appl. Phys. Lett. **95**, 131903 (2009).
[14]J. Simon, N. T. Pelekanos, C. Adelmann, E. Martinez-Guerrero, R. Andre, B. Daudin, L. S. Dang, and H. Mariette, Phys. Rev. B **68**, 035312 (2003).
[15]P. Bhattacharya, M. Zheng, and J. Hinckley, Appl. Phys. Lett. **97**, 251107 (2010).
[16]A. D. Andreev and E. P. O'Reilly, Phys. Rev. B **62**, 15851 (2000).
[17]J. Simon, Y. Cao, and D. Jena, Phys. Status Solidi C **7**, 2386 (2010).
[18]M. Sugawara, K. Mukai, and H. Shoji, Appl. Phys. Lett. **71**, 2791 (1997).
[19]C. Adelmann, B. Daudin, R. A. Oliver, G. A. D. Briggs, and R. E. Rudd, Phys. Rev. B **70**, 125427 (2004).

Downloaded 28 Jan 2013 to 129.74.113.138. Redistribution subject to AIP license or copyright; see http://apl.aip.org/about/rights_and_permissions